Journal of Petroleum Science and Engineering 69 (2009) 239–246

Contents lists available at ScienceDirect

Journal of Petroleum Science and Engineering

journal homepage: www.elsevier.com/locate/petrol

Research paper

Viscous creep in room-dried unconsolidated Gulf of Mexico shale (I): Experimental results

Chandong Chang [a,*], Mark D. Zoback [b,1]

[a] Department of Geology, Chungnam National University, Daejeon, 305-764, South Korea
[b] Department of Geophysics, Stanford University, Palo Alto, CA 94305-2215, USA

ARTICLE INFO

Article history:
Received 12 September 2008
Accepted 27 August 2009

Keywords:
creep
compaction
shale
viscoplastic

ABSTRACT

Laboratory experiments reveal that room-dried unconsolidated Gulf of Mexico (GOM) shale from the South Eugene Island field exhibits pronounced viscous creep behavior under both hydrostatic pressure and triaxial compressive stress. In all tests, the shale exhibits a lack of creep (and nearly negligible strain recovery) when unloaded, suggesting that the creep strain is best considered as viscoplastic deformation. Following application of a step-change in pressure or stress, creep compaction is considerably more significant than that which occurs instantaneously, indicating that the process of shale compaction is largely dependent on the viscoplastic deformation of the frame. Ultrasonic velocity measurements also demonstrate that the contribution of creep to the evolution of dynamic properties is significantly larger than that associated with incremental loading. Dynamic bulk moduli are similar to static moduli especially at high pressures at which pores and cracks are closed. Interestingly, in the hydrostatic compression tests the creep behavior of the shale is different above and below ~30 MPa confining pressure. Above 30 MPa, the amount of creep strain that occurs in 6 h is approximately constant with equal pressurization steps, indicating a linear viscous rheology. Below 30 MPa, the amount of creep increases linearly as pressure is raised in constant incremental steps, indicating a nonlinear viscous rheology. A qualitatively analogous behavior was also observed under differential stress conditions. In a companion paper (Chang and Zoback, in prep) we examine constitutive laws that describe the viscoplastic shale deformation.

1. Introduction

Compaction of sediments is one of the most fundamental geological processes in the evolution of sedimentary basins such as the Gulf of Mexico. Physical and mechanical properties including porosity, permeability and compressibility of sediments evolve as a result of both compaction and diagenetic processes.

It is well known that the compaction of sediments is time-dependent. Laboratory experiments have shown that such time-dependent deformation is evident in a wide variety of sediments and sedimentary rocks (Cogan, 1976; Rongzun et al., 1987; Dudley et al., 1994; Ostermeier, 1995; among others). The mechanism of time-dependent deformation in such materials has been attributed either to pore fluid expulsion under drained condition (Cogan, 1976; Karig, 1993; Hornby, 1998) or to pore pressure redistribution under undrained condition (Holzer et al., 1973; Jones and Wang, 1981). Laboratory experiments, however, show that time-dependent deformation is also evident in dry unconsolidated reservoir sands, which is manifested by creep and stress relaxation under conditions of constant stress and constant strain, respectively (Chang et al., 1997; Hagin and Zoback, 2004a,b, 2007). Also, the field of soil mechanics recognizes plastic creep, also referred to as secondary consolidation. The mechanism responsible for such viscous behavior appears to be related to load-bearing intergranular clay and mica.

In this study we consider time-dependent compaction of shales, which are more common than sands in the Gulf of Mexico. Obviously it is beneficial to study shale in its native state, but it is quite difficult to study the mechanical properties of water-saturated shales because of their extremely low permeability and the dependence of permeability on effective stress (Kwon et al., 2001). Time-dependent deformation of shale is usually attributed to a redistribution of pore water pressure as stress conditions change, i.e., it is considered to be a transient process associated with pore pressure equilibration (Jones and Wang, 1981; Mese and Tutuncu, 1996; Hornby, 1998).

As noted above, time-dependent deformation is an inherent property of dry unconsolidated reservoir sands due to the existence of secondary materials such as clay and mica. Intuitively, dry frame deformation of shale would be expected to exhibit even more prominent creep deformation as shales contain more clay minerals than sands. The main objective of the present laboratory study is to investigate the static and dynamic behavior of time-dependent

* Corresponding author. Tel.: +82 42 821 6430; fax: +82 42 823 5636.
E-mail addresses: cchang@cnu.ac.kr (C. Chang), zoback@stanford.edu (M.D. Zoback).
[1] Tel.: +1 650 725 9295; fax: +1 650 725 7344.

0920-4105/$ – see front matter © 2009 Elsevier B.V. All rights reserved.
doi:10.1016/j.petrol.2009.08.018

deformation of a Gulf of Mexico shale with an emphasis on creep compaction. While a more complete behavior would be obtained by superposing pore pressure effects on that of the dry frame, we believe that isolation of the mechanical properties of the dry frame of shale from pore fluid effects can provide insight into the physics of shale compaction. In a companion paper (Chang and Zoback, in prep) we utilize the experimental data to find a theoretical model that can best describe the creep behavior of the shale.

2. Sample description and experimental procedure

The shale samples used in our experimental study were prepared from cores (102 mm diameter) extracted from a measured depth of 2390 m (true vertical depth of 2260 m) of the deviated Pathfinder well in South Eugene Island Block 330, offshore Louisiana, Gulf of Mexico (Anderson et al., 1994). The original core samples were contained in aluminum tubes, cut by half, wax-coated, and reposited in a chilled and humidified condition for more than 5 years, to preserve in situ lithologic features. For further information about the history of core, refer to Losh (1998). The shale is weak, unconsolidated and very fine-grained (average grain size less than 10 μm), with a composition of more than 50% clay, 30% quartz, and some minor amount of feldspar and plagioclase (Losh et al., 1999). Before we used the cores for experiments, the wax coating was removed and the shale cores in the aluminum tubes have been exposed to the air for more than 2 years. Intermittent bedding planes are observed that are tilted at 40–50° from the core axis. Initial porosity of the room-dried samples, measured using a Boyles' law porosimeter, was $27 \pm 3\%$. Density, determined from measurements of mass and volume of prepared specimens, was 1.86 ± 0.03 g/cm^3.

The unconsolidated shale tends to adsorb moisture in the air (with a relative humidity of ~50%) and thus has a small amount of water in the pores. While the interlayer water in clay is taken to be part of the mineral, it is important to estimate the amount of free water. The pore water content was estimated by oven-drying the shale at 70 °C and monitoring bulk weight loss due to evaporation of pore water. We estimated a pore water content to be 15–20% of pore space (or 4–6% of shale volume). The moisture may affect, to some extent, the deformation of the shale by wetting clays. Because the amount of pore water is considerably smaller than the volume of the pore space, however, we assume that pore pressure effects are virtually negligible in our experiments, even after maximum compaction.

Although there were some desiccation cracks due to drying that formed predominantly along the preexisting bedding planes, the cores were generally in good shape. In order to successfully make test specimens, we had to avoid any evident desiccation cracks. Since the shale cores were very friable, specimen preparation required much care. Cylindrical specimens (25.4 mm diameter, 38–50 mm long) were prepared by manually drilling the core such that the specimen's long dimension was aligned with the core axis. The specimens were jacketed with a heat-shrinkable thin polyolefin tube and securely sealed between two core holders (25.4 mm diameter) to prevent permeation of confining fluid. Two vertical linear variable differential transducers (LVDT) mounted on the core holders provide measurements of axial displacement along two diametrically opposite sides of the specimen as it is compressed; an LVDT directly attached to the jacketed specimen with the guidance of a ring fixture was used to monitor radial displacement. A *P*-wave transducer and a pair of mutually perpendicular *S*-wave transducers were installed on each core holder for ultrasonic velocity measurements. The transducers have a center frequency of 1 MHz. All experiments were conducted in a pressure vessel at ambient temperature.

Our main experimental program consisted of monitoring creep deformation under hydrostatic confining pressure that increased in steps. Fig. 1 shows two typical loading paths used in the hydrostatic pressure tests. Pressure was increased in a stepwise pattern from 10 up to 50 MPa in steps of 5 MPa. Loading rates were 5 MPa/min. During each hold period, the pressure was kept constant for at least 6 h while axial and lateral displacements were continuously recorded, which were later converted to volumetric strain. Fig. 1a shows one type of test, in which pressure was monotonically increased in 5 MPa steps to a peak pressure (this case 30 MPa) and then decreased monotonically in steps. Note that appreciable creep strain accompanied loading steps, while no time-dependent strain accompanied unloading steps. Fig. 1b shows a different type of test, in which pressure was intermittently decreased during loading in order to examine the recovery deformation with lower pressure levels. In all tests, considerable creep strain accompanied the loading steps but negligible creep strain accompanied unloading.

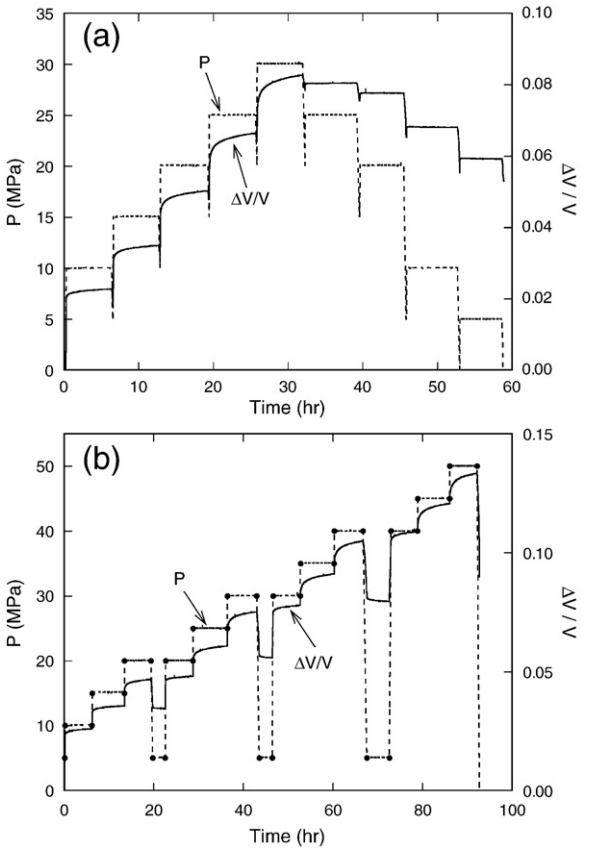

Fig. 1. Two typical loading paths used for the hydrostatic pressure experiments. Pressure (P) was raised in steps of 5 MPa. At each step, pressure was kept constant for at least 6 h during which the volumetric creep strain ($\Delta V/V$) was monitored. Prior to each step, a quick decrease and increase of pressure was applied to isolate the characteristic behavior of creep at the constant pressure level and to prevent superposition of creep from the previous step. Deformation was also examined at lowered pressures obtained by intermittent unloading. Dots in (b) indicate the points where ultrasonic velocities (V_p and V_s) were measured.

We also conducted creep experiments under differential stress conditions. In this type of test (Fig. 2), a hydrostatic pressure of 18 MPa was first applied, followed by stepwise increases in axial differential stress (axial stress minus confining pressure) from 2.7 to 11.7 MPa in steps of about 2.5 MPa. Axial creep strain (labeled ε_1 in Fig. 2) was monitored for at least 6 h during each hold period. After the last hold period at 11.7 MPa, the differential stress was lowered in steps. Note that as in the hydrostatic pressure tests, appreciable creep strain accompanied loading steps but there was negligible strain accompanying unloading.

3. Hydrostatic pressure test results

3.1. Creep behavior

In eight hydrostatic pressure experiments, the unconsolidated Gulf of Mexico (GOM) shale exhibited pronounced creep strain during

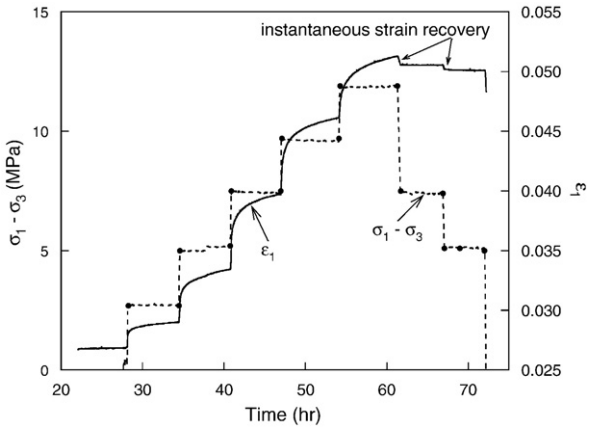

Fig. 2. The loading path used in triaxial compression test. Confining pressure was kept constant at 18 MPa and differential stress (σ_1–σ_3) was raised in steps of about 2.5 MPa. Dots indicate the points where ultrasonic velocities (V_p and V_s) were measured. ε_1 is the strain measured parallel to the sample axis.

loading. Fig. 3 shows typical volumetric creep strain data as a function of time immediately after a loading ramp was halted at a pressure of 30 MPa. For clarity, only the time-dependent strain is shown in this figure. Fig. 3a clearly demonstrates that creep in the dry shale is both a continuous and a significant process. The general form of the creep curve is that primary creep (in which strain rate decreases with time) is followed by steady-state compaction which does not level off (even after 5 days) and is approximately linear with time for the time span we tested. If the creep compaction is assumed to be solely associated with pore space closure, the amount of creep shown in Fig. 3a corresponds to a porosity loss of 1.7%. Plotting creep strain versus log time shows that the primary creep is a logarithmic function of time (Fig. 3b), although the creep will probably level off eventually as the shale continues to consolidate. As Fig. 3 indicates, creep in shale is not just a transient process associated with pore fluid pressure redistribution, but is an inherent property of the dry matrix.

To compare the amount of creep with each step at different pressure levels, Fig. 4 shows the creep part of volumetric strain for each pressure as a function of time (corresponding to the type of test shown in Fig. 1b). The creep data shown in this figure are those measured at the respective pressures during initial loading. While creep occurs at all levels from 10 to 50 MPa, the amount of creep strain varies with pressure magnitude. The amount of creep increases with each 5 MPa pressure step from 10 to 30 MPa. However, as the pressure is increased beyond 30 MPa, the amount of creep strain is relatively constant with each pressure step.

To examine such creep behavior in all of the experiments conducted, we measured the amount of creep after 6 h, and plotted them as a function of pressure (Fig. 5). Different symbols represent tests on different samples. The magnitude of volumetric creep strain after 6 h increases monotonically as pressure is raised from 10 to 30 MPa in 5 MPa steps. At pressure levels above ~30 MPa, the amount of creep with each 5 MPa step is approximately the same (0.0125 ± 0.0015) within the pressure range we tested. A simple relationship between the amount of creep strain and pressure can be expressed with two best-fit lines (indicated by the dashed lines in Fig. 5) for respective pressure ranges below and above 30 MPa. In general, creep behavior of the GOM shale can be characterized by a bilinear dependence on pressure: linearly increasing amounts of creep strain at pressures below 30 MPa and nearly constant amounts at pressures above 30 MPa.

Below 30 MPa, the creep behavior of the GOM shale described above is different from that observed in dry unconsolidated sands. The Lentic sand from GOM (Chang et al., 1997) and a reservoir sand from the Wilmington field (Hagin and Zoback, 2004a,b) exhibited creep strains that are nearly constant for equal increasing steps of pressure, regardless of the pressure magnitude, such that the cumulative creep strain increases linearly with pressure. As shown in Fig. 6, the cumulative creep increases nonlinearly (as $P^{1.7}$) as the pressure increases up to ~30 MPa. At pressures above ~30 MPa, the creep behavior of the shale samples studied here is analogous to that of the unconsolidated sands — the creep strain increment is constant for the same pressure increment, thus defining a linear viscous rheology. The cause of the bilinear creep response to pressure magnitude in the GOM shale is not clearly understood; it may be related either to the in

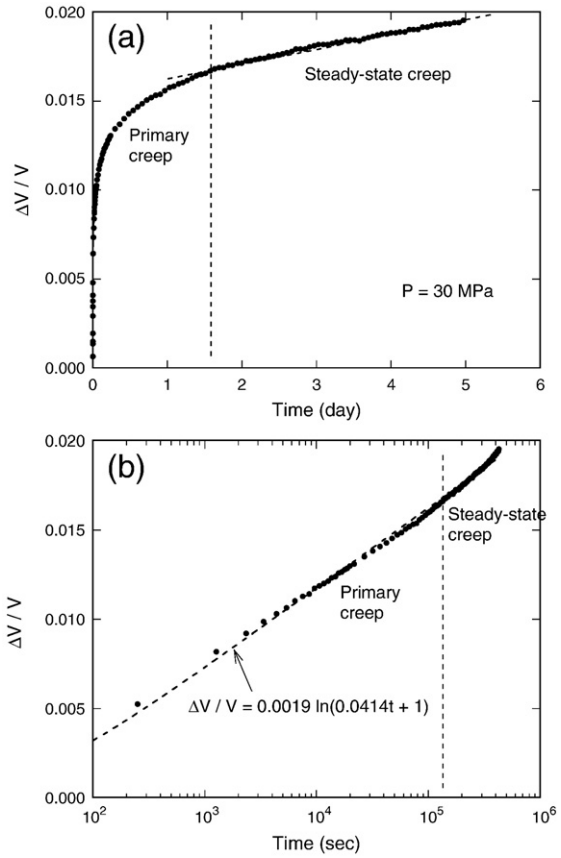

Fig. 3. Volumetric creep strain ($\Delta V/V$) measured at a hydrostatic pressure of 30 MPa for 5 days, showing continuous and significant creep compaction of the dry GOM shale (a). The plot of $\Delta V/V$ and log time reveals that creep strain data can be best-fit by a logarithmic function of time (b).

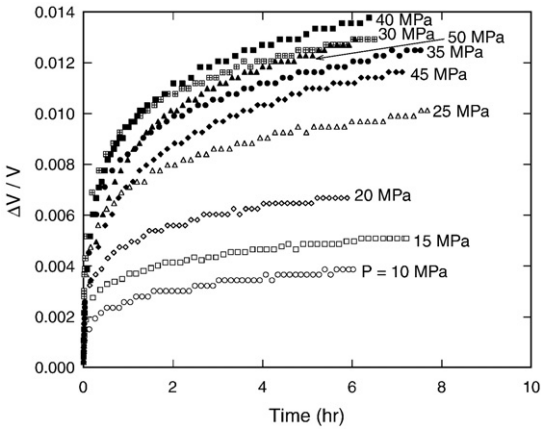

Fig. 4. Volumetric creep strain measured at each different pressure level. The amount of creep varies with the applied pressure: it increases with each 5-MPa pressure step from 10 to 30 MPa, and afterward it is relatively constant as the pressure is increased in equal steps beyond 30 MPa.

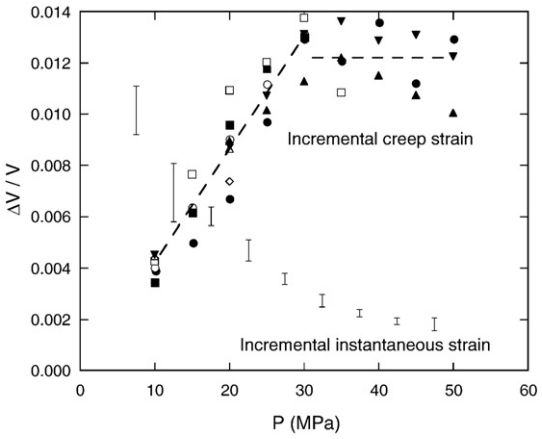

Fig. 5. The amount of volumetric creep strain after 6 h as a function of hydrostatic pressure. Different symbols represent tests on different samples. The amount of volumetric creep strain increases linearly as the pressure is raised in steps of 5 MPa up to 30 MPa, while it is relatively constant above 30 MPa. This result indicates that the pressure-dependence of creep can be characterized by bilinear behavior. It is noted that the creep strain is considerably more significant than the instantaneous strain indicated by vertical lines at pressures above 20 MPa. Note that above 15 MPa the incremental creep strain becomes larger then incremental instantaneous strain (vertical lines).

situ conditions from the depth that the shale core was extracted, or to the internal structure of the shale itself. The bilinear behavior implies, however, that for whatever reason, the mechanism of creep may be different in two pressure ranges.

Fig. 5 compares the amounts of creep strain and instantaneous volumetric strain (vertical lines) induced during each 5-MPa incremental pressure ramp. The amount of instantaneous volumetric strain gradually decreases from about 1% with incremental loading of 5 MPa to about 0.2% as pressure increases due to the stiffening effect of shale at higher pressure. Note that creep strain data shown in Fig. 5 are those for only 6 h. It is noteworthy that creep strain is significantly greater than the instantaneous strain once the sample has compacted at about 15 or 20 MPa, indicating that the time-dependent creep deformation of the dry shale matrix is the dominant mechanism of shale compaction at higher pressures.

We also monitored deformation at constant pressure during unloading steps. In Fig. 7, open symbols indicate changes in strain as a function of time measured at different constant pressures obtained by unloading and subsequent partial reloading (see the constant pressures in the unloading steps in Fig. 1a). Dark symbols represent time-dependent strains observed at constant pressures obtained by unloading without subsequent partial reloading (see the constant pressures in the unloading steps in Fig. 1b). In all of these tests, no creep was observed associated with pressure decrease. We observed a slight time-dependent strain recovery after the shale was unloaded. The amount of strain recovery appears to increase as the pressure drop increases. However, such strain recovery occurs only during the first hour or two, and thereafter the strain stays nearly constant. Note that the amount of time-dependent strain recovery is virtually negligible when compared to that of creep in the increasing loading steps (note that Figs. 4 and 7 are at markedly different scales). Thus, the creep compaction in the GOM shale is nearly irrecoverable deformation and can be characterized as being viscoplastic.

3.2. Dynamic properties

Ultrasonic velocity measurements were carried out in several experiments to investigate the effects of compaction (either time-dependent or instantaneous) on the evolution of the dynamic properties of the shale. *P*- and *S*-wave velocities were measured at the points indicated by dots in Fig. 1b along the loading path. Velocities were obtained by dividing the specimen length at the time of measurement by the arrival time of the transmitted sonic pulses. First arrivals were picked from 50 stacked pulses, which improved the signal to noise ratio. We were able to pick *P*-wave arrivals quite accurately, but it was sometimes difficult to pick the *S*-wave arrival because of the interference with the faster *P*-waves. However, the uncertainty in the measured travel times even for the *S*-waves is usually much less than 1 μs, which results in an error of $\leq 2\%$ in V_s.

Results of a typical experiment are shown in Fig. 8, in which *P*- and *S*-wave velocities, calculated dynamic bulk modulus (K_{dyn}) and Poisson's ratio (ν_{dyn}) are plotted as a function of applied pressure (left column) and as a function of porosity, ϕ (right column). Porosity was calculated based on volumetric strain by assuming that composite particles or grains are nearly incompressible and compaction results solely from decrease in pore space. Since the initial porosity was measured with the sample in a room-dried state (containing some water) and the actual porosity might be slightly different from that shown in Fig. 8, although it would not be significantly so.

It is evident that V_p and V_s generally increase as pressure rises and the shale compacts. V_p increases faster with pressure than V_s, because the ratio stays relatively constant and so does Poisson's ratio (0.26). The magnitude of K_{dyn} increases monotonically with pressure as expected. For the increase in pressure from 5 to 50 MPa, K_{dyn} is almost twice its value at 5 MPa. The magnitude of K_{dyn} increases not only with

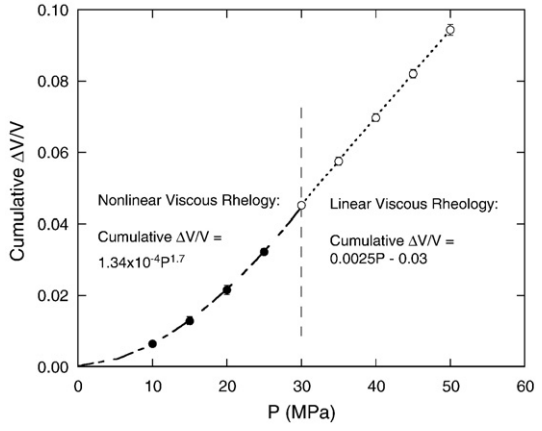

Fig. 6. The cumulative volumetric creep strain after 6 h plotted as a function of pressure in the GOM shale. The viscous rheology can be divided into two ranges based on the pressure-dependence of the cumulative creep strain: Nonlinear viscous rheology below ~30 MPa (dark circles) and linear viscous rheology above ~30 MPa (open circles).

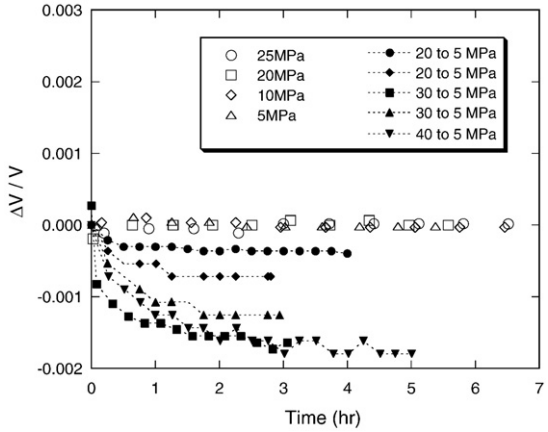

Fig. 7. Volumetric strain as a function of time under different constant pressures obtained by unloading and partial reloading (open symbols), and those under pressures obtained by unloading only (closed symbols). In the former data, no time-dependent deformation was observed. In the latter results, a small amount of strain recovery that lasts about an hour or two was observed.

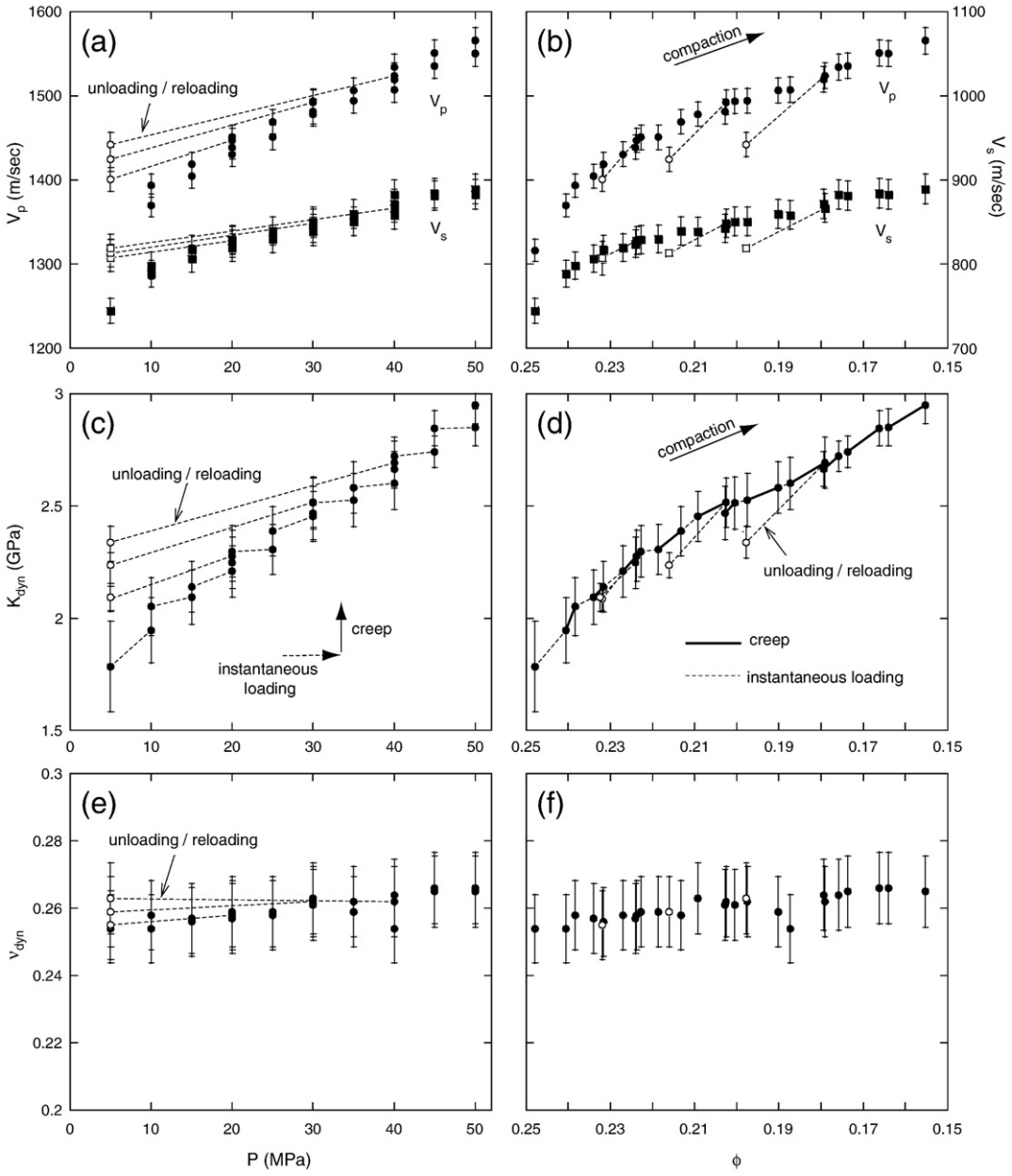

Fig. 8. Ultrasonic velocity measurements carried out in the hydrostatic pressure experiment shown in Fig. 1b. Compressional (V_p) and shear wave (V_s) velocities (a and b), dynamic bulk modulus K_{dyn} (c and d), Poisson's ratio ν_{dyn} (e and f) are plotted as a function of applied pressure P (left column) and porosity ϕ (right column). Dashed lines represent instantaneous loading, unloading, and reloading paths. Solid lines in (d) indicate 6 h creep intervals. Measurements after lowering the pressure are indicated by open symbols.

pressure but also with time (see increase in K_{dyn} for a given pressure in Fig. 8c). The increase in K_{dyn} due to instantaneous loading is significant at pressures lower than 20–30 MPa when the shale is highly compressible. At a higher pressure (>30 MPa), the increase in K_{dyn} due to instantaneous loading becomes negligible, and that due to creep compaction becomes dominant. Even at 50 MPa pressure, the change in K_{dyn} due to creep is about 0.1 GPa for 6 h, which is consistent with those at pressures below. The contribution of time-dependent creep to compaction is clearly shown in the K_{dyn}–ϕ plot (Fig. 8d), in which both porosity reduction and the increase in dynamic modulus are significant during 6 h of creep as marked with solid lines. The slope of K_{dyn}–ϕ lines associated with creep is consistent throughout the experiment, corroborating that the dynamic property evolves proportionally with the shale's compaction state. It appears that as the shale compacts, the major porosity reduction results from time-dependent creep, rather than from instantaneous deformation. Thus, the creep is an intrinsic deformational feature of dry frame of shale, which thus makes it a major process in shale compaction under pressures.

When unloaded, the sample exhibits a high degree of hysteresis in dynamic properties, which is consistent with its mechanical response, as the magnitudes of V_p, V_s and K_{dyn} decrease only slightly upon unloading. Therefore, velocities and dynamic K are affected by loading history. For example, note that their magnitudes at 5 MPa pressure are slightly greater when the sample is unloaded from a higher pressure than when 5 MPa was the highest pressure on the sample. This indicates that the creep deformation is irreversible, again indicating that the compaction of the shale is largely a viscoplastic process. Respective unloading/reloading curves in Fig. 8 are nearly parallel, because the deformation that occurs during unloading is essentially elastic.

The increase in velocities and K_{dyn} value with pressure is typical of shale compaction results of previous studies (Jones and Wang, 1981;

Karig, 1993; Mese and Tutuncu, 1996; Hornby, 1998; among others). Many previous studies, however, ignored shale compaction with time, perhaps because it was considered a transitional effect. As shown in our strain results, time-dependent deformation of the dry frame is a significant viscous process that is mainly responsible for the compaction of shale.

3.3. Comparison of static and dynamic moduli

We measured static bulk moduli along the unloading paths after the shale underwent 6 h creep at respective steps of pressure and plotted them in Fig. 9. The static K (K_{stat}), slope of unloading path, was initially lower than K_{dyn}, but as the pressure increased, the former rose at a faster rate than the latter, and was nearly equal to K_{dyn} at pressures higher than 40 MPa. The ratio of K_{dyn} versus K_{stat} decreases with pressure from 1.26 at 20 MPa to ~1.0 at 50 MPa. It has been suggested that the difference between static and dynamic moduli in dry rocks results from either the presence of pores and cracks (Simmons and Brace, 1965), or the effects of strain amplitude used for measuring deformability (Plona and Cook, 1995). While both reasons may produce the discrepancy between static and dynamic moduli, our results demonstrate that in this shale the difference is greatly reduced at pressures above 40 MPa since pores and cracks are closed under high pressures. Thus, there is a reasonable similarity between dynamic moduli and unloading static moduli in the dry shale at high effective stress.

4. Triaxial compression test results

One of the main reasons to conduct a triaxial creep experiment was to determine if the observations in the hydrostatic tests are reproduced under non-hydrostatic differential stress. The triaxial experiments we conducted were intended to run at a confining pressure of 20 MPa. However, when the pressure was raised to 20 MPa, the sample exhibited continuous creep for more than 20 h. In order to make sure that creep in the triaxial test was produced solely by differential stress, we first raised the confining pressure to 20 MPa, then lowered it to 18 MPa to confirm that the sample did not creep. The loading path after that point used in this experiment is shown in Fig. 2.

Fig. 10 shows creep data for this experiment. The amount of creep strain after 6 h increases as steps of the maximum principal stress (σ_1) are added up from 20.7 to 25.4 MPa. The amount of creep remains constant at the differential stress of 27.5 MPa, and slightly decreases at 29.7 MPa. Thus, the creep behavior of the GOM shale under triaxial compressive stress regime can also be characterized by a bilinear response to the applied differential stress, which resembles qualitatively as shown in Figs. 4 and 5 that is observed in hydrostatic pressure tests.

When unloaded, the shale did not exhibit any creep or strain recovery (see Fig. 2), which is also similar to the case of hydrostatic pressure. Also, the instantaneous strain recovery that occurs during unloading is extremely small, suggesting that creep deformation of the shale due to increasing differential stress is mainly an irrecoverable process and that viscoplastic deformation prevails during compaction under differential stress conditions.

5. Microscopic observations

In order to better understand the micromechanical aspects of shale compaction, we investigated under a scanning electron microscope the microstructure of the shale before and after the creep experiments. Preparation of an unconsolidated shale sample for SEM is difficult in that manipulation of the sample may contaminate its morphology. We carefully cleaned the surface of the sample, so that the undisturbed morphology could be preserved as much as possible. The surface of the sample was then sputter-coated with gold.

Two SEM micrographs are shown in Fig. 11, taken from an undeformed shale and a deformed shale. In the undeformed shale (Fig. 11a), it can be observed that the laminated structures of platy clay minerals are mostly aligned as are the fracture-like voids that appear to be subparallel to the clay lamination. In contrast, the 10 μm (or bigger) irregular-shaped voids are randomly distributed. In the shale deformed under a stepwise pressurization up to 50 MPa (Fig. 11b), lamination of the clay particles is rarely seen. Clay aggregates are tightly packed to blocky lumps, which are typically separated by voids. It should also be noted that the size of typical void spaces is greatly reduced to less than

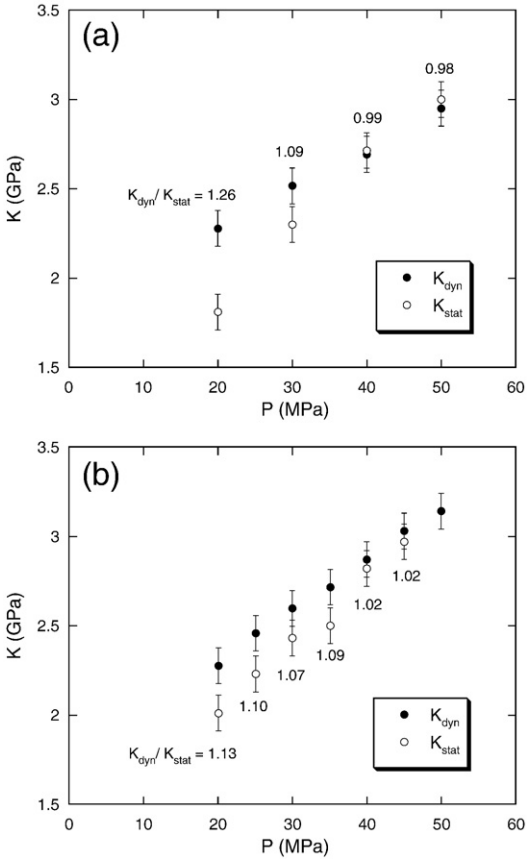

Fig. 9. Comparison of dynamic (K_{dyn}) and unloading static bulk moduli (K_{stat}) in two hydrostatic pressure experiments. The K_{dyn}/K_{stat} ratio at each pressure level is indicated.

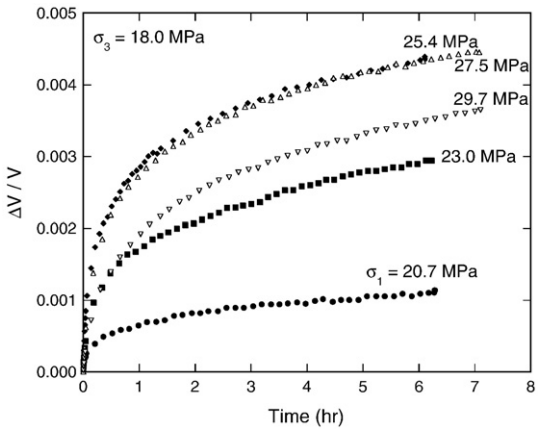

Fig. 10. Volumetric creep strain measured at each maximum principal stress (σ_1) level for a constant confining pressure ($\sigma_3 = 18$ MPa) in triaxial compression test. The amount of creep increases as σ_1 increases up to 25.4 MPa, and thereafter it either stays constant or decreases slightly.

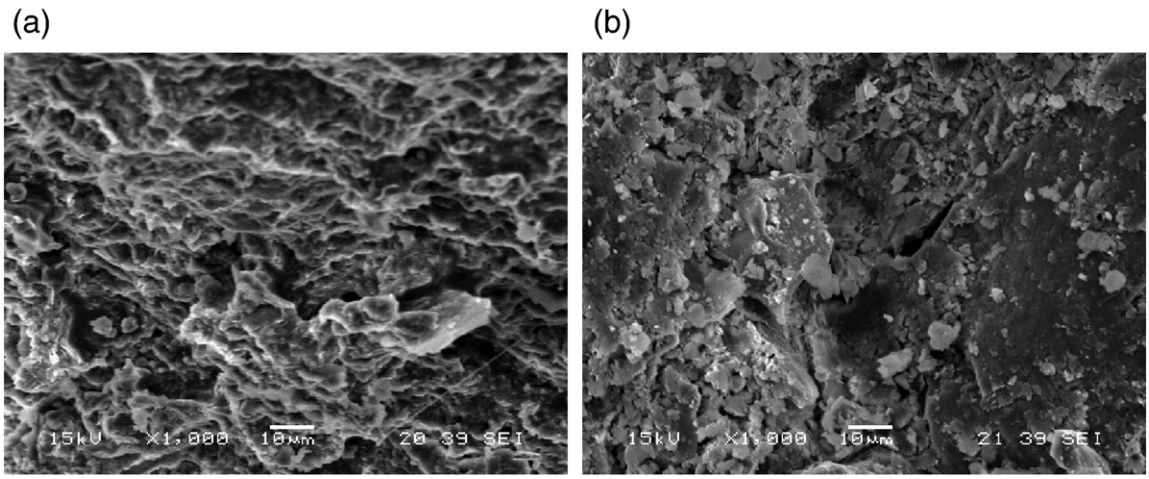

Fig. 11. SEM micrographs of undeformed sample (a) and sample that was subjected to a stepwise increase of pressure from 10 to 50 MPa (b). Difference in clay morphology is evident between these two samples.

10 μm. The major mechanism behind the compaction of the dry shale appears to be the packing of clay and a progressive collapse of pore (void) spaces. Apparently such microscopic features represent an irrecoverable and plastic deformation during shale compaction.

6. Discussion

As we emphasized in the beginning of the paper, the main purpose of this work was to observe the intrinsic creep behavior of shale by isolating the deformation of dry frame from any significant pore fluid interactions. There is an inherent difficulty in choosing test samples suitable for that purpose. Swelling clays such as smectite possess generically interlayer water. Drying a shale almost certainly causes permanent changes to its fabric, because of the sensitivity of clays to their hydration state. On the other hand, saturation brings about a complicated pore fluid interaction during compaction, derived mainly from the extremely low permeable nature of clays. The room-dried shale with the least amount of water content that still makes the sample look shale may not be the perfect selection, but appears to be complementary.

Overall, the amount of creep strain in this shale is much larger than that seen in experiments on uncemented sands from the same well. Hagin and Zoback (2004a) reported that the amount of volumetric creep strain of typical reservoir sand for 6 h immediately after a 5 MPa pressure ramp was about 0.003. In the linear viscous range, the amount of shale volumetric creep strain for the same time period under the same pressure condition is 4 times larger than that of sand. Hagin and Zoback (2004a) showed that creep strain increases as a function of clay content. Since the clay content in the GOM shale is more than 50% and that in the sand was 15% (Hagin and Zoback, 2004a), the proportionally large amount of creep in this rock affirms their supposition that the amount of creep increases with clay content at approximately the same rate.

Another point that we want to discuss is the rheology of the shale. Our experimental results consistently show that creep strain is irrecoverable and time-dependent plastic deformation. During unloading and reloading cycles on over-consolidated shale, the deformation that occurs can be attributed to elastic, because velocities and dynamic moduli recover their values before unloading. During virgin loading, however, the instantaneous portion of the deformation in our tests might incorporate both the elastic and plastic (or viscoplastic) although we used a quite fast loading rate of 5 MPa/min. Any plastic deformation that occurs in that loading can be either pure plastic, viscoplastic, or a combination of both. The most straightforward way to resolve which rheology is more appropriate would be to compare the strain under increasing pressure at an extremely high loading rate (i.e., instantly) and the recovered strain when unloading. If the strain is fully recovered, it will be elastic and the shale will be considered to have an elastic/viscoplastic rheology. If not, the general rheology of the shale will be an elastoplastic/viscoplastic. A clear distinction between these two rheologies was not made in our study. In our companion paper (Chang and Zoback, in prep), however, we assumed that the deformation of the shale is elastic/viscoplastic, because it is simpler and provides a good prediction of shale compaction.

The last point to discuss is that if the creep compaction is irrecoverable, why does the shale experience creep again at pressures below the stress from which the shale was obtained in the well? A rough estimation of the overburden pressure at the depth (TVD = 2260 m) where the shale was recovered can be made based on an assumed vertical stress gradient (23 MPa/km, equivalent of 2.3 g/cm^3 density) and a hydrostatic pore pressure (10 MPa/km). Although we do not have pore pressure information in this well (in fact, there are some traces of high pore pressure evidence; for example, a porosity of 27% at that depth is somewhat high for a hydrostatic pore pressure), this assumed pressure condition may give insight into creep behavior of the shale. Based on the assumed values, an effective overburden pressure was estimated to be about 29 MPa. Thus if we tested rock samples exactly as in situ, the matrix of shale would have not yielded creep at pressures below 29 MPa. However, our shale samples are room-dried and fluid has been removed from pores and cracks. We infer that the viscous creep at pressures below 30 MPa that we observed might result mainly from the collapse of such emptied pores and cracks which in situ would be filled with fluid. Under real conditions at depth, this would not occur since shales are fully saturated and no empty pores exist. We postulate that if the shale has never been subjected to pressure originally, it would yield larger creep strain in the pressure range below 30 MPa than that we observed in our experiments. Only at pressures higher than 29 MPa, the entire shale matrix including pores would begin to creep. Thus, it is inferred that the creep strains above 30 MPa (linear viscous rheology) may represent more realistically viscous characteristic of shale matrix in situ.

7. Conclusions

Our laboratory experiments revealed that room-dried unconsolidated Gulf of Mexico shale exhibits a pronounced time-dependent creep, under both hydrostatic and triaxial loading conditions, whenever it is loaded beyond its previous maximum load. The contribution of creep to shale compaction was significantly larger than that of

instantaneous loading. Porosity loss and increases in dynamic moduli of the shale were observed during creep. The dynamic moduli of the room-dried shale were practically similar to the unloading static moduli, especially when high pressure closes pores and cracks. These results demonstrate that the room-dried frame of the shale has intrinsically time-dependent characteristics, which comprise a major mechanism of shale compaction. The creep strain in the shale is largely unrecoverable with unloading, suggesting that the deformation process is best described as viscoplastic.

The creep behavior in the shale depends on the magnitude of the applied pressure (or stress). The amount of creep after a given time after a constant pressure increment was seen to increase linearly up to 30 MPa. Thus, the total cumulative creep strain increases nonlinearly as pressure increases in this pressure range. When the pressure was increased in the same equal steps beyond 30 MPa, the amount of creep after a given time at a constant pressure level was nearly constant, suggesting that at higher pressure, creep characteristics obey a linear viscous rheology.

The amount of creep strain in shale is significantly larger than that in sands with less clay, which corroborates previous observations that creep strain increases with clay content. Microscopic inspections show that creep in shale appears to be the packing of clay and a progressive collapse of pore spaces.

Acknowledgments

This research was supported by the Stanford Rock and Borehole Geophysics (SRB) Program. We thank Paul Hagin for his assistance with this work. Constructive comments and suggestions from three reviewers greatly enhanced the quality of the paper.

References

Anderson, R.N., Flemings, P., Losh, S., Austin, J., Woodhams, R., 1994. Gulf of Mexico growth fault drilled, seen as oil, gas migration pathway. Oil Gas J. 92, 97–103.

Chang, C., Moos, D., Zoback, M.D., 1997. Anelasticity and dispersion in dry unconsolidated sands. Int. J. Rock Mech. Min. Sci. 34 Paper No. 48.

Chang, C., Zoback, M.D., in prep. Viscous creep in room-dried unconsolidated Gulf of Mexico shale (II): Development of a viscoplasticity model. J. Petrol. Sci. Eng.

Cogan, J., 1976. Triaxial creep tests of Opohonga Limestone and Ophir Shale. Int. J. Rock Mech. Min. Sci. 13, 1–10.

Dudley, J.W., Myers, M.T., Shew, R.D., Arasteh, M.M., 1994. Measuring compaction and compressibilities in unconsolidated reservoir materials via time-scaling creep. Eurock '94, SPE/ISRM International Conference, Delft, Netherlands, pp. 45–54.

Hagin, P.N., Zoback, M.D., 2004a. Viscous deformation of unconsolidated sands; Part 1, time-dependent deformation, frequency dispersion, and attenuation. Geophysics 69, 731–741.

Hagin, P.N., Zoback, M.D., 2004b. Viscous deformation of unconsolidated reservoir sands; Part 2, linear viscoelastic models. Geophysics 69, 742–751.

Hagin, P.N., Zoback, M.D., 2007. Predicting and monitoring long-term compaction in unconsolidated reservoir sands using a dual power law model. Geophysics 72, E165–E173.

Holzer, T.L., Höeg, K., Arulanandan, K., 1973. Excess pore pressure during undrained clay creep. Can. Geotech. J. 10, 12–24.

Hornby, B.E., 1998. Experimental laboratory determination of the dynamic elastic properties of wet, drained shales. J. Geophys. Res. 103, 29,945–29,964.

Jones, L.E.A., Wang, H.F., 1981. Ultrasonic velocities in Cretaceous shales from the Williston basin. Geophysics 46, 288–297.

Karig, D.E., 1993. Uniaxial reconsolidation tests on porous sediments: mudstones from site 897. In: Whitmarsh, R.B., Sawyer, D.S., Klaus, A., Masson, D.G. (Eds.), Proceedings of the Ocean Drilling Program, Scientific Results, vol. 149, pp. 363–373.

Kwon, O., Kronenberg, A.K., Gangi, A.F., Johnson, B., 2001. Permeability of Wilcox shale and its effective pressure law. J. Geophys. Res. 106, 19339–19353.

Losh, S., 1998. Oil migration in a major growth fault: structural analysis of the Pathfinder core, South Eugene Island Block 330, offshore Louisiana. AAPG Bull. 82, 1694–1710.

Losh, S., Eglinton, L., Schoell, M., Wood, J., 1999. Vertical and lateral fluid flow related to a large growth fault, South Eugene Island Block 330 field, offshore Louisiana. AAPG Bull. 83, 244–276.

Mese, A.I., Tutuncu, A.N., 1996. An experimental investigation for relationship between physicochemical and acoustic properties of pure kaolinite and Pierre shale. SEG Annual Meeting Expanded Technical Program Abstracts with Biographies, pp. 1695–1698.

Ostermeier, R.M., 1995. Deepwater Gulf of Mexico turbidites; compaction effects on porosity and permeability. SPE Formation Evaluation 10, 79–85.

Plona, T.J., Cook, J.M., 1995. Effects of stress cycles on static and dynamic Young's moduli in Castlegate sandstone. In: Daemen, J.J.K., Schultz, R.A. (Eds.), Proc. 35th U.S. Rock Mech. Symposium, pp. 155–160.

Rongzun, H., Zuhui, Z., Jingen, D., 1987. The creep characteristics of shale formation and the analysis of its loading on the oil well casing. In: Herget, G., Vongpaisal, S. (Eds.), Proc. 6th Congress Int. Soc. Rock Mech, vol. 6, pp. 137–139.

Simmons, G., Brace, W.F., 1965. Comparison of static and dynamic measurements of compressibility of rocks. J. Geophys. Res. 70, 5649–5656.